A feedback-loop extended stress fiber growth model with focal adhesion formation

Pradeep Keshavanarayana[a,*], Martin Ruess[a], René de Borst[b]

[a]*School of Engineering, University of Glasgow, United Kingdom*

[b]*Department of Civil and Structural Engineering,University of Sheffield, United Kingdom*

Abstract

Contractile cells play a prominent role in the adaptive nature of biological tissues. Contractility is mainly attributed to the growth of the tension dependent actomyosin bundles called stress fibers within the cytoskeleton. Stress fibers extend along the length of the cell and end at focal adhesions on the cell membrane. At the focal adhesion junctions on the cell membrane the integrin proteins are capable of sensing the environment, thereby making the cellular behavior dependent on the cell supporting substrate. It has been observed that the growth of stress fibers influences focal adhesions and vice-versa, resulting in a continuous cross-talk between different processes in the cell. Recent experiments have shown that cells subjected to uni-axial cyclic loading, depending on the substrate properties reorient themselves in a direction away from the loading direction, exhibiting strain avoidance.
Mathematical models are important to understand the dependence of the cellular behavior on the substrate properties along with feedback mechanisms and are further used in designing in-vitro experiments. The coupling of the models for stress fibers and focal adhesions results in a non-linear bio-chemo-mechanical problem. In this contribution, we present the positive influence of the growth of focal adhesions along with a mechanosensitive feedback loop on the stress fiber growth and further reveal the characteristics of the re-orientation process due to cyclic loading. We use a non-linear Hill-type model to capture the growth of the active stress involved in the evolution law for the stress fibers and a thermodynamical approach to model the focal adhesions. A highly stable and reliable monolithic solution scheme is used to solve the governing system of coupled equations. Finally, we validate our simulation results with experimental results in regard to different loading conditions.

Keywords: cell motility, fiber re-orientation, feedback loop, monolithic solution

*Corresponding Author
Email addresses: p.keshavanarayana.1@research.gla.ac.uk (Pradeep Keshavanarayana), martin.ruess@glasgow.ac.uk (Martin Ruess), r.deborst@sheffield.ac.uk (René de Borst)

Contents

1 Introduction **3**

2 A bio-chemo-mechanical cell model **4**
2.1 Modeling of stress fibers 5
2.2 Modeling of focal adhesions 9
2.3 Calcium growth and feedback 12

3 Governing equations and monolithic solution scheme **14**
3.1 Governing equations 15
3.2 Weak formulation 16
3.3 Material data and discretization 16
3.4 Monolithic solution approach 17

4 Numerical results **19**
4.1 External force induced focal complex formation 20
4.2 Interdependence of focal adhesions and stress fibers 21
4.3 Stress fiber reorientation 24

5 Summary and conclusions **27**

1. Introduction

Cells are the fundamental units of all cellular organisms. Groups of cells, constituting tissues, have the ability to reform their structure and properties depending on external cues. The dynamic reorientation of tissues can be seen as an accumulation of responses of individual cells. Understanding the cellular properties is imperative in order to develop artificial tissue type materials. In recent times, with improvements in experimental techniques, mechanisms leading to constant change in mechanical and bio-chemical properties of cells have been understood fairly well [1]. Though not all the involved processes are understood, a broad consensus has been reached on how the energy conversion results in cellular motility, constantly changing the shape and size of cells as a means of response to stimulus. In addition to the internal reactions, cells exhibit a continuous interaction with the extra-cellular matrix (ECM) allowing them to sense the stimulus exerted by the ECM. As a consequence of chemical reactions and interactions with the ECM, variations in cellular mechanical properties have been found during diseased states such as malaria [2], asthma [3] and cancer [4] among many other deadly diseases.

When responding to stimuli, cells contract, resulting in stress evolution. Contraction is responsible for the continuous reorganization of the internal skeletal structure of the cell called the cytoskeleton. At the sub-cellular scale, the actin-cytoskeleton is responsible for maintaining the shape and size of the cell [5]. Specifically, actin filaments form a cross-bridge complex with the myosin II motor proteins to form stress fibers that carry the contractile stresses within the cell. Although many similarities can be drawn between stress fibers in non-muscular cells such as tissue fibroblasts and sarcomeres in muscle cells, stress fibers are less ordered and reorient themselves in a highly dynamic fashion [6]. The stress fibers usually extend over the length of the cell, Fig. 1(a) and end on the cell membrane at the cell-ECM junctions called focal adhesion (FA), Fig. 1(b).

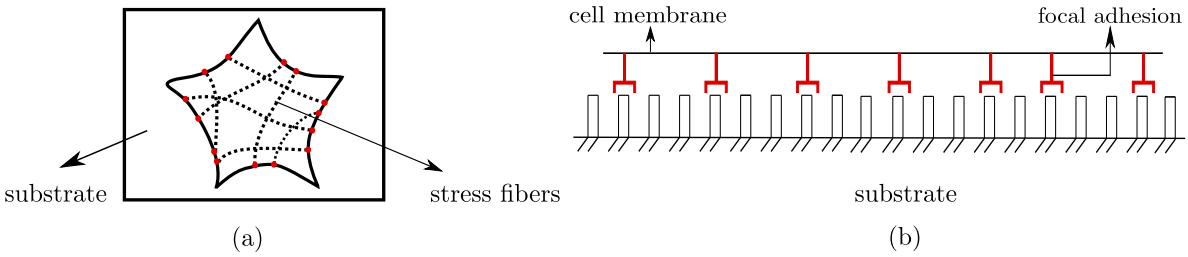

Figure 1: (a) Top view of the cell placed on a substrate showing the stress fibers within the cell and focal adhesion on the cell membrane. (b) Side view of the cell showing focal adhesion bonding the cell membrane to the substrate.

The FA complexes are responsible for developing the required connection between the actin cytoskeleton and the ECM, which is accomplished through the mechanically functioning proteins called integrins [7]. Thus, integrins at FAs are responsible for the cell's interactions with its surroundings, thereby establishing the difference between living cells and dead cells.

The in-vitro experiments performed on cells alone are insufficient to explain the in-vivo behavior which is mainly due to the cross link between the internal cytoskeleton and the ECM. Hence, mathematical models describing the cell behavior become indispensable to predict the bio-chemo-mechanical properties. Moreover, they allow to reveal the sensitivity of each of the different mechanisms in order to understand better the overall cell response and to support the design of further experiments.

Recent studies have emphasized that the properties of the cell-supporting substrate used in experiments influence the growth and reorientation of stress fibers, which affects the focal adhesion growth, thereby forming a cyclic chain of reactions. Furthermore, the existing models do not consider the coupling effect between FAs and stress fibers during cyclic loading experiments. In this article, we extend the existing works and present a phenomenological model where both, focal adhesion and stress fiber growth, have been coupled by a feedback loop, bridging the influence on the other. The formulation results in a coupled system of equations which we solve using a monolithic approach. We provide numerical evidence that the feedback-loop extension is a vital property to reproduce experimental observations on focal adhesion growth. We also show that our feedback-loop extended model is capable of simulating the dynamic coupling of focal adhesions and stress fibers through a stimulating calcium signaling process. Finally, we apply the model to simulate the stress fiber orientation in a cell subject to cyclic loading in one and two dimensions in order to reveal the effects of a changing amplitude.

The paper is structured as follows: in section 2 we briefly review experimental and numerical studies of biomechanical cell models. We then introduce the models and assumptions used for the representation of stress fibers and focal adhesions, respectively, and their coupling through the introduced feedback loop. In section 3 we derive the mathematical model including the governing differential equations, a weak formulation, a corresponding discretization and a monolithic solution approach for the coupled governing system of equations. In section 4, we demonstrate the validity and performance of the model by a number of numerical experiments. Finally, in section 5 we summarize the main findings and draw conclusions.

2. A bio-chemo-mechanical cell model

In the past, a large number of experiments have been conducted to investigate the behavior of cells under different loading and environmental conditions. Atomic force microscopy [8] and micropippete aspiration [9] were used to determine the mechanical properties of different types of cells. Experiments have also revealed the dependence of the cellular behavior on substrate properties [10–12]. In [12–14] it was found that a cyclic stretching of cells caused the stress fibers to reorient themselves either in the direction of the applied load or away from it, depending on the precise external conditions.
In addition to experimental progress, mathematical models have been developed over the past two decades which allow a numerical prediction of static and dynamic properties of cell

motility and cell remodeling. This opens the door for more detailed, comprehensive studies. The ability of numerical simulations to explain cellular behaviour such as contractility, motility and growth is mainly driven by the model capabilities to represent non-linear constitutive relations and the stress-strain dependence on the chemo-mechanical loading. Discrete models as the tensegrity model of Ingber [15] or the cellular solid model of Satcher et al. [16] were used to simulate cytoskeletal properties. Recently, models have been proposed which suggest a catch-bond mechanism to model stress fibers which provides a multiscale approach to cell contractility [17, 18]. Other models favor a continuum approach which allow for the simulation of stress fiber reorientation subjected to various types of cyclic loading [19–24]. Many models consider the stress fibers coupled with FA formation [25–27], since focal adhesions play an important role with regard to the response of cells. A few models rely purely on focal adhesions [28, 29]. Here, we follow a continuum approach which we stepwise introduce and extend in the following by a feedback-loop mechanism.

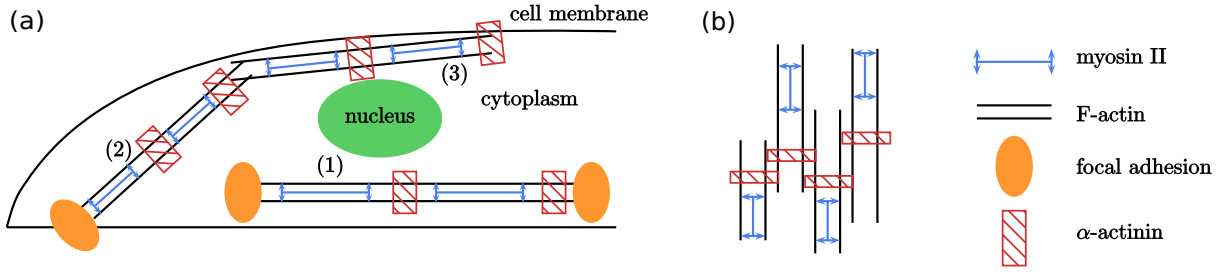

Figure 2: (a) types of stress fiber: ventral stress fibers (1), dorsal stress fibers (2) and transverse arcs (3). The stress fibers are classified based on their location, their chemical constituents remain the same; (b) cross-bridge between *alpha*-actinin, F-actin, and myosin II.

2.1. Modeling of stress fibers

Actin filaments present in cytoplasm are connected to each other by α-actinin proteins to form an actin bundle. Different bundles are cross linked by myosin II proteins forming stress fibers [30]. Based on their sub-cellular location, stress fibers are classified into three types: ventral stress fibers, dorsal stress fibers and transverse arcs, as shown in Fig. 2(a).

Ventral stress fibers are the most common stress fibers within a cell which originate and terminate at focal adhesions. Dorsal stress fibers are attached to the focal adhesion at one end while transverse arcs are found to disassemble near the nucleus of the cell. With this background, the following three assumptions are considered for the development of an appropriate stress fiber model:
(i) the internal stresses have to be transferred to its external surroundings to ensure the mechanical equilibrium of the cell. Hence, the stress fibers must be connected to the ECM at the focal adhesions which can happen only in ventral stress fibers. The mathematical models therefore can simulate ventral stress fibers only. On the other hand, actin staining experiments show all types of stress fibers and therefore we assume sufficient actin and myosin proteins to be available to form ventral stress fibers, which we refer to simply as

stress fibers. Extending this hypothesis, we further assume that during stress fiber reorientation, the reduction of the stress fiber concentration in one direction does not influence the concentration in other directions. That is, the formation of stress fiber in one direction does not curtail the availability of actin to form stress fibers in other directions.
(ii) The sarcomeric model of contraction results in the contraction of muscle fibers by shortening the actomyosin bridge [30], whereas, in case of non-sarcomeric models as shown in Fig. 2(b), the α-actinin acts as a blockade for the bridge formation. Hence, the solution for the stress fiber growth during contraction is obtained by allowing rapid cycles of dissociation and re-association of α-actinin to actin filaments [31]. Thus, an increase in contractile stress leads to reduced dissociation rather than a direct increase in association.
(iii) The free calcium ions present in cytoplasm play an important role in stress fiber contractility as observed in [32], [33].

Based on these assumptions we formulate the following stress fiber growth model in terms of a directional stress fiber concentration rate, cf [19]:

$$\dot{\eta}(\phi) \;=\; \begin{cases} (1-\eta(\phi))\, C\, k_f - (1-\kappa)\, \eta(\phi)\, k_b & \text{if } \kappa < 1 \\ (1-\eta(\phi))\, C\, k_f & \text{if } \kappa \geq 1 \end{cases} \tag{1}$$

where,

$$\kappa \;=\; \frac{\sigma^a(\phi)}{\sigma_0(\phi)} \tag{2}$$

is the ratio of active stress $\sigma^a(\phi)$ in the stress fiber due to the actomyosin bridge to the isometric stress $\sigma_0(\phi)$ and where

$$\sigma_0(\phi) \;=\; \eta(\phi)\, \sigma_{max} \tag{3}$$

with σ_{max} being the maximum stress allowed in the stress fiber. The stress fiber concentration at an inclination angle ϕ is denoted with $\eta(\phi)$, $(0 \leq \eta(\phi) \leq 1)$. Furthermore, C represents the calcium concentration available for the contractility within the cytoplasm and k_f and k_b are rate constants related to the association and dissociation of stress fibers, respectively. We further assume $\eta(\phi) = 0$ at $t = 0$ to be an appropriate initial condition.
From eq. (1) we can conclude the following principal behavior for the growth model: (i) as the concentration of stress fiber increases, the rate of stress fiber association reduces, (ii) the association of stress fibers is directly dependent on the calcium concentration, (iii) if the active stress in the stress fiber is less than the isometric stress, an increase in the active stress prevents further dissociation of stress fibers and (iv) if the active stress is greater than or equal to the isometric stress, we assume that no further dissociation is possible, and hence the dissociation part becomes zero.

The high structural and behavioral similarities between muscle sarcomeres and stress fibers justifies the use of models which were derived for the growth of stresses in muscle fibers to

describe the fundamental relations between kinematic and static components. The state of stress in these models is found to be dependent on both, the state of strain [34] and the strain rate [35]:

$$\frac{\sigma^a}{\sigma_0} = f(\varepsilon)\, g(\dot{\varepsilon}) \tag{4}$$

where $f(\varepsilon)$ and $g(\dot{\varepsilon})$ are two independent functions depending on the state of strain (ε) and the corresponding strain rate ($\dot{\varepsilon}$), respectively.

Stress-strain rate relation: The function $g(\dot{\varepsilon})$, which represent the growth of stress in the

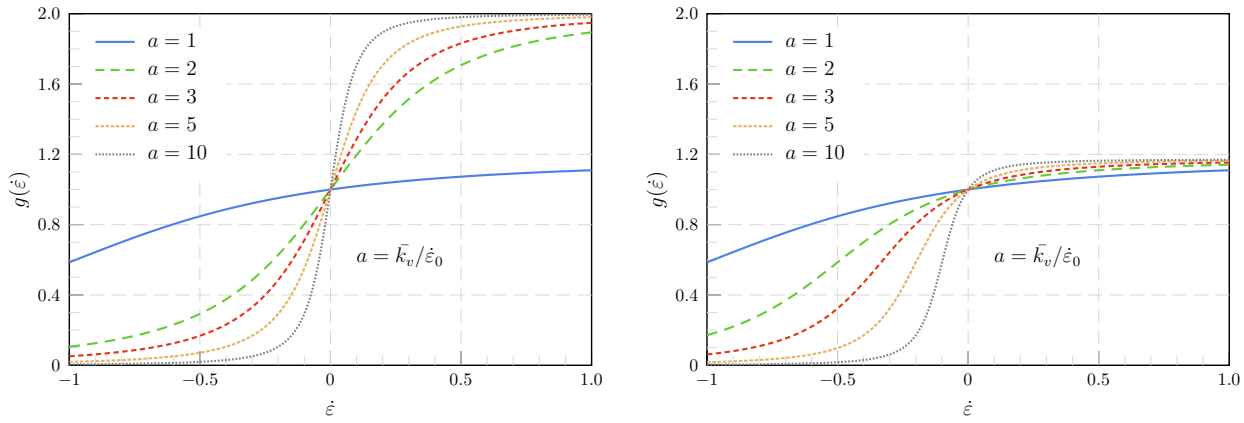

(a) expansion parameter $S_{exp} = 0$ **(b)** expansion parameter $S_{exp} = 1$

Figure 3: Influence of the expansion parameter S_{exp}, equation (5), on the Hill-type stress fiber growth function $g(\dot{\varepsilon})$.

stress fibers due to the strain rate is assumed to follow a Hill type growth. Here, we use a modified, smooth non-linear version of the Hill model [35] based on the linear piecewise continuous model used in [19, 21]:

$$g(\dot{\varepsilon}) = \frac{1}{1 + \frac{S_{exp}}{\sqrt{({S_{exp}}^2+1)}}} \left(1 + \frac{\bar{k}_v \frac{\dot{\varepsilon}}{\dot{\varepsilon}_0} + S_{exp}}{\sqrt{\left(\bar{k}_v \frac{\dot{\varepsilon}}{\dot{\varepsilon}_0} + S_{exp}\right)^2 + 1}} \right) \tag{5}$$

where S_{exp} is an expansion parameter which introduces a non-uniform compression of the curve for $S_{exp} > 0$, as shown in Figure 3. The expansion parameter becomes significant only when the cell is subjected to cyclic loading [20, 21].
The Hill constant $\bar{k}_v$ is a dimensionless constant for the dissociation of contraction and $\dot{\varepsilon}_0$ is a parameter representing the strain rate sensitivity. From eq. (5) we observe the following overall model behavior:

(i) the function g tends to zero when the strain rate increases to minus infinity:

$$\dot{\varepsilon} \to -\infty : \qquad g(\dot{\varepsilon}) \to 0 \tag{6}$$

This implies that the stress fiber dissociates and the stresses cannot grow when the stress fiber is subjected to a very high negative strain rate.
(ii) as the strain rate increases positively, $g(\dot{\varepsilon})$ converges towards a stationary point

$$\dot{\varepsilon} \to +\infty : \qquad g(\dot{\varepsilon}) \to \frac{2}{1 + \frac{S_{exp}}{\sqrt{({S_{exp}}^2+1)}}} \tag{7}$$

which is a constant greater than or equal to one. The corresponding plateau value depends on the expansion parameter S_{exp} and is equal to 2 for $S_{exp} = 0$. In the numerical examples presented in section 4 we choose $S_{exp} = 0$ when no cyclic loading is applied and $S_{exp} = 1$ when the cell is subjected to cyclic loading.
(iii) For a zero strain rate, i.e. the isometric state, we have for all values of S_{exp}

$$g(0) \;\; = \;\; 1. \tag{8}$$

reducing the model to a purely static model response.

Stress-strain relation: The stress-strain relation can be derived in analogy to the characteristics of cables which are stiff in tension but which have no stiffness in compression. Thus, the stress will drop to zero for an increase of negative strains and will evolve for a positive strain value. In our model we use [20]:

$$f(\varepsilon) = \begin{cases} \exp\left(-\left(\frac{\varepsilon}{\varepsilon_0}\right)^2\right) & \text{if } \varepsilon < 0 \\ \exp\left(-\left(\frac{\varepsilon}{\varepsilon_0}\right)^2\right) + \left(\frac{\varepsilon}{\varepsilon_1}\right)^2 & \text{if } \varepsilon \geq 0 \end{cases} \tag{9}$$

where ε_0 is a decay constant for the contraction when the strain becomes negative and where the constant ε_1 characterizes the passive strain hardening. Following [20] the ratio $\varepsilon_1/\varepsilon_0$ is kept constant at a value of 1.4. For $\varepsilon = 0$, $f(\varepsilon) = 1$, maintaining the unit value at the isometric state.

With eq. (3) and the relations (5) and (9) the active stress follows as

$$\sigma^a \;\; = \;\; \eta(\phi)\, \sigma_{max}\, f(\varepsilon) g(\dot{\varepsilon}) \tag{10}$$

representing the active stress in an individual stress fiber. In order to describe the anisotropic stress fiber contraction within the cell, a 2-dimensional homogenization is used to evaluate

the stress tensor:

$$\boldsymbol{\sigma} = \frac{1}{\pi}\begin{bmatrix}\sigma_{11} & \sigma_{12}\\ \sigma_{21} & \sigma_{22}\end{bmatrix} \tag{11}$$

with

$$\begin{aligned}
\sigma_{11} &= \int_{-\pi/2}^{\pi/2} \sigma^a(\phi)\, cos^2(\phi)\, d\phi \\
\sigma_{12} &= \int_{-\pi/2}^{\pi/2} \frac{1}{2}\sigma^a(\phi)\, sin(2\phi)\, d\phi \\
\sigma_{21} &= \int_{-\pi/2}^{\pi/2} \frac{1}{2}\sigma^a(\phi)\, sin(2\phi)\, d\phi \\
\sigma_{22} &= \int_{-\pi/2}^{\pi/2} \sigma^a(\phi)\, sin^2(\phi)\, d\phi.
\end{aligned}$$

The strain and strain rate along the fiber with inclination angle ϕ are obtained by a similarity transformation in the 2D-plane using the inclined basis vectors:

$$\varepsilon(\phi) = \varepsilon_{11}\, cos^2(\phi) + \varepsilon_{22}\, sin^2(\phi) + \varepsilon_{12}\, sin(2\phi) \tag{12}$$

$$\dot{\varepsilon}(\phi) = \dot{\varepsilon}_{11}\, cos^2(\phi) + \dot{\varepsilon}_{22}\, sin^2(\phi) + \dot{\varepsilon}_{12}\, sin(2\phi). \tag{13}$$

The contractile deformation of the stress fibers is confined by the passive resistance of the cytoskeleton through the intermediate filaments. For simplicity, the material offering such resistance is assumed to be isotropic and the stress-strain behavior as linear elastic,

$$\sigma^p = E\,\varepsilon \tag{14}$$

where σ^p denotes the passive stress, E is the passive elastic modulus and ε is the axial fiber strain. In three dimensions, total stress can be written as the sum of active and passive stress components:

$$\Sigma_{ij} = \sigma^a_{ij} + \left(\frac{E\nu}{(1-2\nu)(1+\nu)}\,\varepsilon_{kk}\delta_{ij} + \frac{E}{1+\nu}\varepsilon_{ij}\right) \tag{15}$$

where ν denotes the Poisson ratio and δ_{ij} is the Kronecker delta.

2.2. Modeling of focal adhesions

Focal adhesions are made up of multi-protein structures, which contain integrins that form a mechanical link between the cytoskeleton and the extra cellular matrix [29]. Experiments reveal that integrins exist in two conformational states: (i) a low affinity or bent state and

(ii) a high affinity or straight state. Integrins in the straight state are assumed to form a bond with the substrate, while integrins in the bent state are free. Thus, for modeling purposes, the high affinity integrins can be assumed to represent the focal adhesions which form a bond between the cell and the substrate as shown in Fig 4.

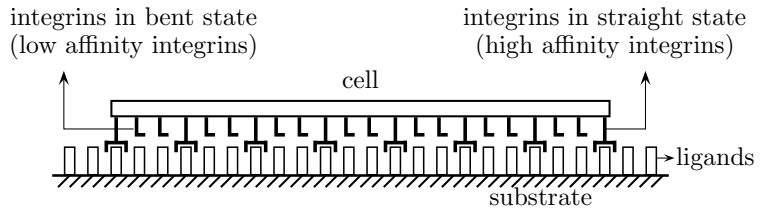

Figure 4: Low and high affinity integrins in a 1-D cell attached to a soft substrate where the high affinity integrins are assumed to represent the focal adhesions.

The modeling of the focal adhesions follows a thermodynamical approach represented by the chemical potential for low and high affinity integrins [27, 36]:

$$\mu_L = \mu_L^R + k\,T\ ln\left(\frac{\xi_L}{\xi_0}\right) \tag{16}$$

$$\mu_H = \mu_H^R + k\,T\ ln\left(\frac{\xi_H}{\xi_0}\right) + \Phi - F\,\Delta \tag{17}$$

where μ_L and μ_H are the chemical potentials of the low and high affinity integrins, respectively. Furthermore, μ_L^R and μ_H^R are the reference chemical potentials while ξ_L and ξ_H are the concentrations of the low and high affinity integrins, respectively. The Boltzmann constant is denoted by k and the absolute temperature by T. Furthermore, ξ_0 denotes the reference number of integrins [36]. A comparison of (16) and (17) reveals two additional terms in (17) which result from the fact that, due to bonding with a bearing substrate the potential of the high affinity integrins depends on the tensile force they are subjected to [29]. The bond energy is denoted with Φ. With $(F\,\Delta)$ we denote the work done by the bond while being stretched by Δ. Thus, the force exerted by the bond can be evaluated from the bond energy Φ as

$$F = \frac{\partial \Phi}{\partial \Delta} \quad . \tag{18}$$

The model is based on the following assumptions and relations:

- at thermodynamic equilibrium, the chemical potentials of high and low affinity integrins must be equal. Thus,

$$\mu_H = \mu_L \tag{19}$$

  will result in the inter-conversion of integrins from a low to a high affinity state and vice versa. From (16), (17) and (19), the relation between high and low affinity integrins

reduces to

$$\frac{\xi_H}{\xi_L} = \exp\left(\frac{\mu_L^R - \mu_H^R - \Phi + F\,\Delta}{k\,T}\right). \tag{20}$$

- In the FA models of [27, 36], low affinity integrins were assumed to move along the cell membrane which was modeled by a diffusion equation, satisfying zero-flux boundary conditions. The explicit modeling of the diffusion of low affinity integrins violates the conservation of the total number of integrins within the domain. To remedy this deficiency, we neglect diffusion of low affinity integrins. This is reasonable since the diffusion of low affinity integrins does not contribute to the focal adhesion formation through inter-conversion of integrins. Thus, the conservation of the total number of integrins reduces to

$$\xi_0 = \xi_L + \xi_H \tag{21}$$

where ξ_0 is the total number of integrins in the system which is inter-converted between low affinity and high affinity integrins based on their potential. Substitution of eq. (21) into (20) gives:

$$\xi_L = \frac{\xi_0}{1+\alpha} \tag{22}$$

$$\xi_H = \frac{\xi_0 \alpha}{1+\alpha} \tag{23}$$

with

$$\alpha = \frac{\xi_H}{\xi_L} \quad . \tag{24}$$

- the bond energy Φ in the high affinity integrins is assumed to depend on the stretch quadratically:

$$\Phi = \frac{1}{2}\lambda_s\,\Delta_e^2 \tag{25}$$

where $\Delta_e = \sqrt{\Delta_1^2 + \Delta_2^2}$ is the effective stretch, and Δ_1 and Δ_2 represent the stretches in the x_1 and x_2 directions, respectively, while λ_s represents the bond stiffness so that:

$$F = \lambda_s\,\Delta \quad . \tag{26}$$

- the stretch is related to the displacement as

$$\dot{\Delta} = \begin{cases} \dot{u} & \Delta_e \leq \Delta_{max} \\ 0 & \text{otherwise} \end{cases} \tag{27}$$

where Δ_{max} is the maximum allowable stretch in the stress fibers.

In summary, the model reflects the following behavior: integrins subjected to stimuli, whether in the form of mechanical forces or bio-chemical signals, respond either by the formation or dissociation of focal adhesions. If more focal adhesions are needed to maintain equilibrium, low affinity integrins are converted to high affinity integrins through the thermodynamic equilibrium. The total number of integrins in the system is preserved.

2.3. Calcium growth and feedback

Essential processes of a living cell such as mechanosensing or the growth of stress fibers involve multiple proteins such as *FAK*, *Src*, *Talin*, *Vinculin*, *Rho* and their interactions. Though the behavior of each of these individual proteins is clear to some extent, the combined actions and its effect on the cellular properties are not understood completely. Integrins on the cell membrane receive signals from the ECM resulting in the activation of *inositol triphosphate* (IP3) messenger molecules. The IP3 molecules diffuse through the cytoplasm and attach themselves to the receptors on the endoplasmic reticulum and release free calcium ions (Ca^{2+}). The Ca^{2+} ions thus available in cytoplasm bind to the calcium modulated protein calmodulin and activate the calmodulin dependent protein kinase (CaMKII), which leads to the activation of the small GTPase enzyme RhoA [37]. Further, RhoA and its downstream effector Rho-associated kinase (ROCK) act as principal mediators for the growth of tension in the cytoskeleton [38]. ROCK is found to attach to myosin phosphatase, inhibiting phosphatase activity and thereby increasing myosin phosphorylation. In addition, they are also attached to LIM Kinase (LIMK) which generates actin monomers, together promoting stress fiber contractility through the formation of an actomyosin bridge complex [39], cf Fig. 2(b).

The formed actomyosin complex will generate stress fibers which lead to focal adhesion growth [40]. Simultaneously, the focal adhesion growth manipulates the RhoA signaling and hence the growth of stress fibers. In [41] it was shown that cells placed in suspension showed an increased level of RhoA, but low phosphorylation and hence low stress fibers. This indicates that the mechanisms in the cell are interconnected and there exists a feedback loop between the focal adhesion formation, the calcium concentration, the myosin phosphorylation and the stress fiber generation as illustrated in Fig. 5. The concentration of calcium which is released from the endoplasmic reticulum stores into the cytoplasm is regulated by mitochondria, thus keeping its concentration under a limit.

Due to different time scales of each of these processes, periodic spikes are observed over time in the calcium concentration [42] which are lost again with an increasing degree of

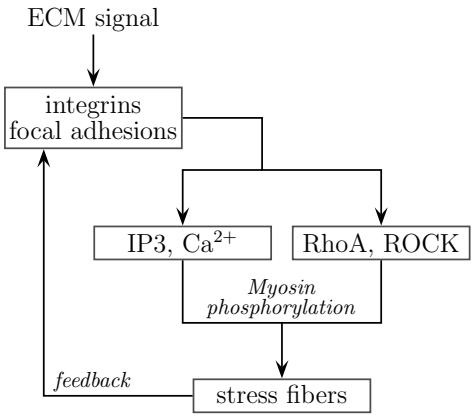

Figure 5: Signaling feedback loop within a cell.

stimulation of the receptor. Since we assume in our model that the focal adhesions are fully grown and play the role of receptors, we assume a high receptivity and neglect the spiking behavior of calcium.

In Fig. 6, we depict the generation of calcium within the cytoplasm and illustrate the following mechanism: (i) the receptor-initiated hydrolysis of phosphatidylinositol 4,5-bisphosphate (PIP2) by phospholipase C (PLC) results in the formation of inositol 1,4,5-triphosphate (IP3) and diacylglycerol. (ii) IP3 is further hydrolysed to be released as IP2, while some of IP3 molecules attach themselves to the calcium gates at the endoplasmic reticulum (ER). This attachment opens the calcium channels and releases calcium to the cytoplasm. (iii) In order to maintain the calcium concentration within the cytoplasm, the ER absorbs some of the calcium ions in the cytoplasm, while some of the calcium passes the cell membrane through mitochondria. Thus, calcium present in the cytoplasm results in the myosin phosphorylation, which, in turn, leads to the formation of stress fibers and focal adhesion as described in section 2.2.

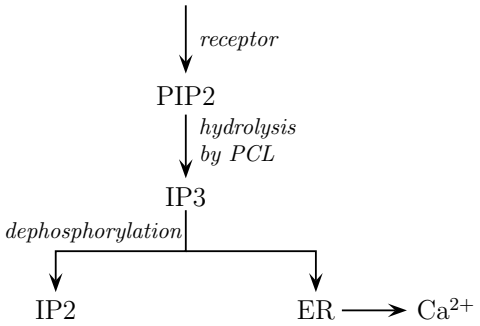

Figure 6: Generation and release of calcium.

From a mechanobiology point of view, the generation of calcium within the cytoplasm can be considered as a two-step process, where the generation of IP3 is modeled by a reaction-diffusion equation followed by a rate equation representing the calcium growth. In this

regard, we exploit a calcium growth model which includes a mechanosensitive feedback [26]:

$$\dot{S} \;=\; m_s\, k\, T\, \frac{\partial^2 S}{\partial x_i^2} - k_d\, S + \frac{\alpha_c}{b}\, max(0, \dot{\xi}_H) - S\, \dot{\varepsilon}(\phi) \tag{28}$$

where S is the IP3 concentration, $x_i\,(i = 1, 2)$ is the spatial coordinate and m_s is the mobility of IP3. The reaction terms involve the rate constant k_d for the hydrolysis of IP3 into IP2, a non-dimensional proportionality constant α_c and the rate value $\dot{\xi}_H$ representing the change of the FA concentration. The strain rate of the stress fibers at an angle ϕ is represented by $\dot{\varepsilon}(\phi)$.

From equation (28), it follows that some of the produced IP3 is diffused through the cytoplasm to reach the endoplasmic reticulum gates and some of the produced IP3 is hydrolysed to IP2 without having effect on the calcium generation. The growth of IP3 is affected only when new focal adhesions are formed but remains unaffected when focal adhesions are dissociated.

The growth of calcium depending on the available IP3 can be written as [26]:

$$\dot{C} \;=\; \lambda_f\, \frac{S}{S_0}\, (1 - C) - \lambda_b\, C \tag{29}$$

where C represents the calcium concentration and λ_f and λ_b are the forward and backward rate constants, respectively. The boundary condition is chosen to be $\nabla S = 0$ on all boundaries of the analysis domain and the initial condition at $t = 0$ is chosen as $S(0) = S_0$ and $C(0) = 0$. From (29) it follows that $C = 0$ when $S = 0$. This implies that there is no calcium without IP3, and hence no phosphorylation.

The calcium concentration C obtained from eq. (29) is used in eq. (1) to evaluate the stress fiber concentration. Thus, equations (28) and (29) together represent the feedback loop that exist within the cell, where calcium concentration is affected by the focal adhesion formation which is governed by the mechanical equilibrium of the cell. The resulting calcium affects the stress fiber formation which changes the focal adhesion concentration and thereby closes the loop.

3. Governing equations and monolithic solution scheme

Based on the fundamental mechanical and bio-chemical properties derived in section 2 we derive the governing equations describing the cell contractility phenomenon. We propose an iterative monolithic solution scheme for the mixed set of algebraic equations including a bio-chemical feedback loop and present its algorithmic structure and further solution aspects.

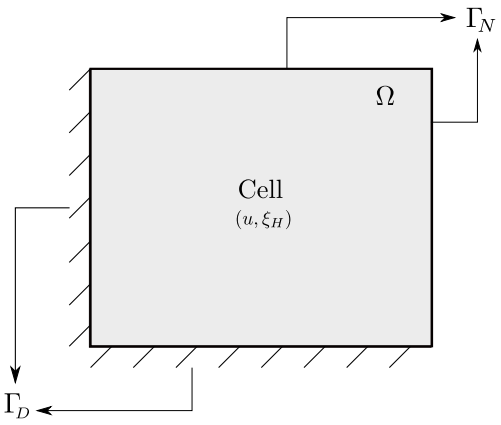

Figure 7: Solution domain Ω with Dirichlet boundary Γ_D and Neumann boundary Γ_N, solved for the state variables u and ξ_H.

3.1. Governing equations

With the definition of the total stress (15), cf. section 2.1, the mechanical equilibrium of the cell, over the domain shown in Fig. 7, follows as:

$$b\,\Sigma_{ij,j} = T_i \quad \text{in } \Omega \tag{30}$$

$$u_i = u_{i0} \quad \text{on } \Gamma_D \tag{31}$$

where u_i and u_{i0} denotes the displacement coordinates and corresponding prescribed boundary values on the Dirichlet boundary Γ_D, where the Neumann boundary Γ_N is assumed traction free and where $\Gamma_D \cup \Gamma_N = \Gamma$ denotes the total boundary of the domain Ω. Thickness of the cell is denoted by b. Cell is subjected to a domain load due to focal adhesions

$$T_i = \xi_H\, F_i \quad \text{in } \Omega \tag{32}$$

where ξ_H is the concentration of the high affinity integrins and F_i is the force exerted by the bond. The initial conditions at $t = 0$ are assumed to be $u(0) = 0$, $\Delta(0) = 0$, $\sigma^a(0) = 0$, and $\varepsilon(0) = 0$. Applying these initial conditions the factor α, eq. (24), which represents the ratio (ξ_H/ξ_L), simplifies to

$$\alpha_0 = \exp\left(\frac{\mu_L^R - \mu_H^R}{k\,T}\right) \tag{33}$$

and hence the high and low affinity integrin concentrations at $t = 0$ reduce to

$$\xi_{H_0} = \frac{\xi_0\,\alpha_0}{1+\alpha_0} \tag{34}$$

$$\xi_{L_0} = \frac{\xi_0}{1+\alpha_0} \tag{35}$$

respectively. Thus, the concentration of focal adhesion lies between ξ_{H_0} and 1. The overall problem reduces to finding the solution of equilibrium (30) and updating the high affinity integrin concentration (23), subject to the initial and boundary conditions.

3.2. Weak formulation

Calcium growth model: The calcium growth model, equation (29), requires the solution of the reaction-diffusion equation (28) describing the generation of the IP3 concentration. Multiplying eq. (28) with a test function δS and performing integration by parts on the analysis domain Ω yields the weak form:

$$\begin{aligned}\int_\Omega \dot{S}(\delta S)\, d\Omega = &- m_s\, k\, T \int_\Omega \frac{\partial S}{\partial x_i}\frac{\partial(\delta S)}{\partial x_i}\, d\Omega - k_d \int_\Omega S\,(\delta S)\, d\Omega - \dot{\varepsilon} \int_\Omega S\,(\delta S)\, d\Omega \\ &+ \frac{\alpha_c}{b}\, max(0, \dot{\xi}_H) \int_\Omega \delta S\, d\Omega \end{aligned} \tag{36}$$

The solution of eq. (36) yields the IP3 concentration which is used to integrate equation (29) providing the requested calcium concentration. Finally, the stress fiber concentration is computed by solving eq. (1) using the calcium concentration. The calcium concentration and the stress fiber concentration are based on first order ordinary differential equations, cf equations (29) and (1), respectively, which are solved using an embedded Runge-Kutta method. This method is a single-step approach which approximates the solution of the initial value problem considering two Runge-Kutta estimates of different order to allow for a control of the truncation error with adaptive stepsize [43].

Active stress model: Weak form of the mechanical equilibrium can be obtained by multiplying (30) with the test function δu_i and performing integration by parts, which is solved subject to symmetry displacement boundary conditions:

$$\begin{aligned} -b \int_\Omega \Sigma_{ij}\,(\delta u_{i,j})\, d\Omega - \int_\Omega \xi_H\, F_i\,(\delta u_i)\, d\Omega \;&=\; 0 \\ \wedge\; u_i \;&=\; u_{i0} \quad \text{on } \Gamma_D \end{aligned} \tag{37}$$

where b denotes the cell thickness, where total stress Σ_{ij} follows from (15). Similarly, the weak form for high affinity integrin concentration ξ_H, (23), is obtained as:

$$\int_\Omega \xi_H\,(\delta\xi_H)\, d\Omega - \int_\Omega \xi_0\, \frac{\alpha}{1+\alpha}\,(\delta\xi_H)\, d\Omega \;=\; 0 \tag{38}$$

3.3. Material data and discretization

The values for the set of parameters of the calcium growth and the stress fiber model are listed in Table 1 and were kept constant throughout all computations. The material parameters of the stress fibers were taken from literature [20, 26, 36], while all other model

parameters were set to match the time scale of the simulated experiments. Further model parameters used for particular simulations are given in their respective sub-sections.

For the numerical solution of the calcium growth model, eq. (36) is discretized using bilinear finite elements. The unknown IP3 concentration S is interpolated using linear shape function R_i as:

$$S = \sum_i R_i S_i \qquad i = 1 \ldots, N \tag{39}$$

where S_i represents the unknown nodal IP3 concentration, leading to the linear system of equations:

$$\mathbf{K}_{ss}\, \mathbf{S} = \mathbf{F}_s \tag{40}$$

where, $\mathbf{K}_{ss}$ and $\mathbf{F}_s$ are stiffness matrix and force vector respectively obtained from (36). Solving (40) yields the nodal IP3 concentration $\mathbf{S}$.For the complete discretization of eq. (36), we refer the reader to the Appendix.

Similarly, the governing integral equations (37) and (38) are discretized in terms of a finite element model using bilinear elements. The unknown displacement and concentration fields, respectively, are interpolated using linear shape functions R_k as

$$\mathbf{u} = \sum_i R_i U_i \qquad i = 1 \ldots, 2N \tag{41}$$

$$\xi = \sum_j R_j \Xi_j \qquad j = 1 \ldots, N \tag{42}$$

where U_i and Ξ_j are the unknown nodal displacements and the nodal high affinity integrin concentrations, respectively. The derivatives of the virtual work integrals with respect to the unknown nodal displacement values and the concentrations yield the governing algebraic equations of the monolithic approach:

$$\begin{bmatrix} \mathbf{K}_{UU} & \mathbf{K}_{U\Xi} \\ \mathbf{K}_{\Xi U} & \mathbf{K}_{\Xi\Xi} \end{bmatrix} \begin{bmatrix} \mathbf{U} \\ \mathbf{\Xi} \end{bmatrix} = \begin{bmatrix} \mathbf{F}_U \\ \mathbf{F}_\Xi \end{bmatrix} \tag{43}$$

where, $\mathbf{K}_{UU}$, $\mathbf{K}_{\Xi\Xi}$, $\mathbf{K}_{U\Xi}$ and $\mathbf{K}_{\Xi U}$ are the stiffness contributions according to (37) and (38), and the corresponding coupling matrices. Furthermore, the external load vector $\mathbf{F}_U$ represents the applied traction load according to (18) and (37) and the load vector $\mathbf{F}_\Xi$ stems from the second term of (38). Agai, the discrete with all sub-matrices and sub-vectors of the monolithic system of equations are presented in the Appendix.

3.4. Monolithic solution approach

The mixed chemo-mechanical problem formulation results in a coupled governing system of equations which we solve with a monolithic solution scheme. The solution provides the

parameter	symbol	value
Passive elastic modulus	E	0.08 kPa
Poisson's ratio of cell	ν	0.3
Tensile strength of stress fibers	σ_{max}	20 kPa
Maximum stretch	Δ_{max}	130e-9
Focal adhesion bond stiffness	λ_s	0.015e-3
Boltzmann constant	k_b	1.38e-23 m^2 kg s^{-2} K^{-1}
Temperature	T	310K
Difference in reference chemical potential between high and low affinity integrins	$\Delta\mu$	$5k_bT$
Reference integrin concentration	ξ_0	5000e+12 integrins/m^2
IP3 mobility constant	m_s	1e+10 s/kg
IP3 diffusion proportionality constant	α_s	10
IP3 de-phosphorylation rate constant	k_d	5e-4 s^{-1}
Reference IP3 concentration	s_0	1000e18 molecules/m^3
Forward rate constant of Calcium release	λ_f	1.0 s^{-1}
Backward rate constant of Calcium release	λ_b	0.5 s^{-1}

Table 1: Material parameters

cell displacement field as well as the high affinity integrin concentrations. In each solution step we solve simultaneously for the unknowns, and update the approximate solution with a Newton-Raphson scheme. The convergence criteria of the iteration is based on displacements only, which is justified since the governing equation for the integrin concentration is dictated by the stretch. The criterion has the form:

$$|\delta^i| \quad \leq \quad \varepsilon_r \, |\delta^t| \tag{44}$$

where $|\delta^i|$ denotes the maximum change in the displacements of successive iterations and $|\delta^t|$ denotes the maximum change in the displacements over each complete time step. We choose $\varepsilon_r = 0.5$ to achieve a reasonably balanced convergence rate. The algorithm of the stepwise iterative solution scheme is presented in Algorithm 1. We use the following notation:

- the time step increment is denoted by Δt
- the i^{th} step of the equilibrium iteration is denoted by a right upper index i
- an index t refers to the converged solution of the last time step

- the unknown nodal displacements and concentrations are summarized in $\boldsymbol{V} := [\boldsymbol{U};\boldsymbol{\Xi}]$.

Data: model geometry and material parameter values, cf Table 1
Result: nodal displacement field and high affinity integrin concentrations at time $t = t_{end}$

% *model setup and initialization*
setupAnalysisModel();
$t = 0$;

% *incremental time step loop*
while $t < t_{end}$ **do**

% *evaluate calcium concentration using an embedded Runge-Kutta method, eq.* (29)
C = calciumConcentration($S, S_0, \lambda_f, \lambda_b$);

% *evaluate stress fiber concentration using an embedded Runge-Kutta method, eq.* (1)
η = stressFiberConcentration($\lambda_f, \lambda_b, C, \kappa, \phi$);

% *Newton-Raphson iteration until stopping criteria, eq.* (44)*, is satisfied*
while $\delta^i > \varepsilon_r \, \delta^t$ **do**

% *solution of the governing system of eq.* (43)*, quantities refer to time* $t + \Delta t$
$\mathbf{K}^{i-1} \, \Delta\mathbf{V}^i = \mathbf{F}_{int}^{i-1} - \mathbf{F}_{ext}^{i-1}$;

% *solution update in time step* $t + \Delta t$
$\mathbf{V}^i = \mathbf{V}^{i-1}$ - $\Delta\mathbf{V}^i$;

% *update of the convergence parameters*
δ^i = max(abs($\mathbf{U}^i$ - $\mathbf{U}^{i-1}$));
δ^t = max(abs($\mathbf{U}^i$ - $\mathbf{U}^t$));

end
% increment time step
$t = t + \Delta t$;
end

Algorithm 1: Monolithic solution scheme for the analysis of the chemo-mechanical cell response.

4. Numerical results

In this section, we test the performance of the framework in terms of accuracy and reliability of the chemo-mechanical model. We further demonstrate the need for the feedback loop to ensure a correct analysis of the cell response. To this end, we consider a 1D numerical

experiment to demonstrate the focal adhesion growth subject to the introduced feedback-loop. We simulate the direct dynamic relation of stress fibers and focal adhesions by calcium signaling with and without the feedback-loop to reveal that the feedback mechanism is necessary in order to be able to reproduce experiments reliably. Furthermore, we use a 2D in-vitro contraction experiment to validate our model and to study the stress fiber re-orientation under cyclic loading. We highlight the importance of the new model for an improved simulation of the stress fiber re-orientation and focal adhesion formation.

4.1. External force induced focal complex formation

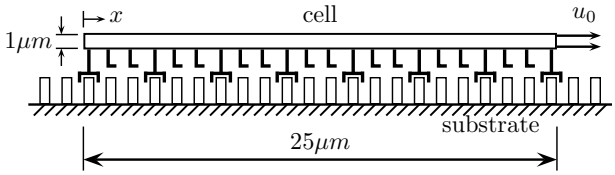

$\bar{k}_v$	=	1.0	Hill constant
k_f	=	$1.4e-4\,s^{-1}$	rate of formation
k_b	=	$1.4e-5\,s^{-1}$	rate of dissociation
ε_0	=	$1.0e-2$	strain constant
$\dot{\varepsilon}_0$	=	$1.0e-2\,s^{-1}$	strain rate sensitivity

Figure 8: 1D cell representation with prescribed displacement as a function of time.

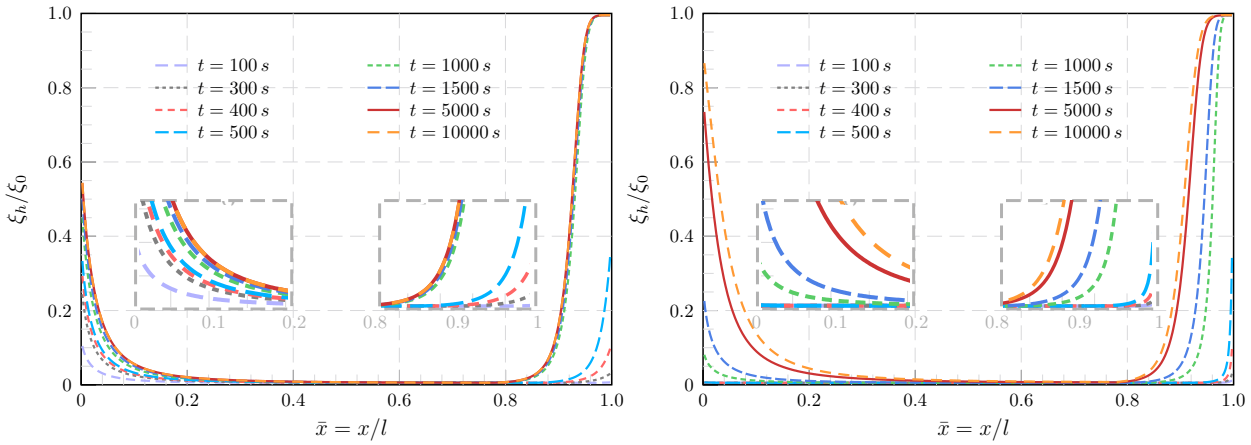

(a) *without* feedback loop **(b)** *with* feedback loop

Figure 9: Focal adhesion growth matches the experimental observations only upon the application of a feedback loop.

In a series of optical trap experiments *Galbraith et al.* have revealed 'The relationship between force and focal complex development' [44] and shown that an external force acting on the cell results in the focal adhesion complex formation, even when placed on a ligand-coated surface where the cell is unable to develop focal adhesion complexes by itself. Furthermore,

it was observed that Vinculin, which is a marker for both focal complex and focal adhesion, did not change over tens of minutes, confirming the applicability of our model. A tight coupling of external forces and a focal adhesion formation was shown earlier in [45] and is studied in the following numerical example taken from [26].

We consider a 1-D cell which is placed on an infinite rigid substrate and which is subjected to a prescribed displacement u_0 at one end of the cell, as depicted in Fig. 8. We use the material parameters specified in Table 1 and additional model parameters as specified in Fig. 8. Pursuant to the experimental and numerical observations, we expect the focal adhesions to form initially near the end where the force is prescribed and eventually to form at the other end of the cell due to its mechano-sensitive properties.

We have simulated the numerical experiment with and without feedback loop to demonstrate its importance for a reliable and correct result. For the case where no feedback mechanism was considered we used an ad-hoc decaying calcium signal $C = exp(-t)$ to trigger a calcium release needed for the focal adhesion formation [19]. Without the feedback mechanism the focal adhesion concentration increases initially at the free left end of the cell while the force was applied at the right end, cf Fig. 9(a). Even at the loaded end of the cell a growth of focal adhesions was observed only after a time greater than 500s. Conversely, an almost immediate growth was apparent at the left end of the cell. Hence, the simulated development of an initial focal adhesion growth on the left end of the cell contradicts the experimental observations.

Next, we replaced the ad-hoc calcium signal with the feedback loop as given by eqs. (28) and (29). The effect of the feedback loop is illustrated in Fig. 9(b). The concentration of free calcium changes within the cytoplasm which affects the growth of stress fibers and hence the focal adhesions. Initially, the focal adhesion concentration was higher at the right end of the cell where the prescribed force was applied. Eventually, focal adhesions grew on the other end of the cell as well. At the state of equilibrium, the focal adhesion concentration was highest at the boundary of the cell, matching the experimental observations [46].

4.2. Interdependence of focal adhesions and stress fibers

With the next numerical experiment, we use the feedback-loop extended model to demonstrate the dynamic coupling of stress fibers and focal adhesions. To this end, we simulate the effect of ROCK inhibition which will reveal a direct suspension of stress fiber growth and thus, of focal adhesion growth.

ROCK (Rho-associated protein kinase) is an enzyme which plays a major role in the stress fiber formation, cf. section 2.3. In [10] it was shown that ROCK inhibition diminishes the myosin phosphorylation within the cytoplasm and hence reduces the measured tractions by almost 50%. This reduces the cytoskeletal tension and hence the stress fiber concentration. It was also found by vinculin staining that the ROCK inhibitor results in a reduced concentration of focal adhesion. Further, it was observed in suspended cells that the activity of RhoA is high, but the concentration of stress fibers is low due to reduced phosphorylation

[41]. Furthermore, adhesion is required for the GTP-bound RhoA to activate ROCK [38]. In summary, these experimental observations show that by suspending the growth of stress fibers through ROCK inhibition, the focal adhesion growth is suspended. Based on the inter-dependence between calcium, stress fibers and focal adhesion as illustrated in 4.1, we hypothesize that stress fiber growth is suppressed by inhibition of focal adhesion growth.

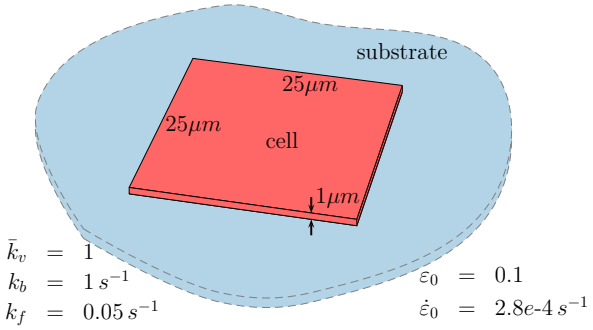

Figure 10: Square cell model on an infinite substrate.

In the model, the strong link between ROCK and myosin phosphorylation is brought about by calcium signaling through the feedback loop as given by eqs. (28) and (29). The phosphorylation leading to stress fiber growth is activated by a signaling calcium concentration which we derive from reference concentrations of IP3 and ξ_H, respectively. The stress fiber growth leads to a new equilibrium state for the cell, which again changes the focal adhesion concentration and thus completes the feedback loop.

When the focal adhesion is kept constant, either indirectly by ROCK inhibitors or by keeping the cell in a suspension, the calcium signal decays and prevents further growth of stress fibers which indicates the absence of phosphorylation. Alternatively, by inhibiting the growth of focal adhesion, we prevent an increase in the traction force $\xi_H F$. This affects the mechanical equilibrium and results in reduced contractile stress, and hence an increased stress fiber dissociation.

The influence of focal adhesion on stress fibers is considered with a two-dimensional cell placed on an infinite substrate depicted in Fig. 10. In addition to the parameters shown in the figure, we use the material parameters according to Table 1. Two different conditions are taken into consideration: with the first condition we allow the focal adhesion to grow as a force-dependent mechanism, following the thermodynamic equilibrium of (19), while in the second condition, the focal adhesion is maintained at its initial value, eq. (34). The second condition represents the behavior of cells subjected to ROCK inhibition or cells in a suspended state.

The results of the stress fiber growth analysis are depicted in Fig. 11. The stress fiber concentration of cells under contraction considering ROCK inhibition drops due to the absence of focal adhesion. In contrast, when focal adhesion growth is not restrained, stress fibers are formed significantly. Similar results have been observed using different bond-catchiness

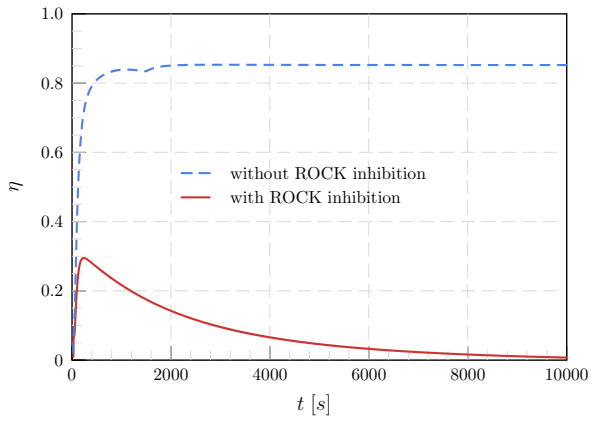

Figure 11: Stress fiber growth over time: Comparison of stress fiber growth when the cells are subjected to ROCK inhibition and without ROCK inhibition.

values in [17]. Due to the different time scales of focal adhesion and IP3 growth, the stress fiber growth without ROCK inhibition exhibits a small kink around $t = 2000s$. Here, we are interested in the equilibrium state of the cell only and do not attempt to change the time scales of these processes. Thus, by preventing the focal adhesion growth, whether by ROCK inhibition, or by placing the cell in suspension, which further affects the calcium signal, stress fiber growth is restrained as seen in Fig.11 . In Fig. 12 we depict the growth of focal adhesion on the square test cell, which is not subjected to ROCK inhibition, and hence focal adhesion is allowed to grow. The focal adhesion growth is higher on the boundary of the cell than at the center which fully corresponds to the observed experimental growth pattern presented in [46].

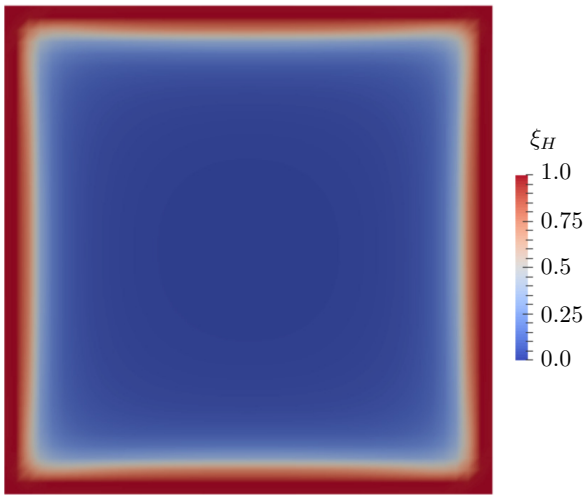

Figure 12: Focal adhesion growth on a square cell.

4.3. Stress fiber reorientation

In the next step we illustrate the potential of the model to predict the different stress fiber alignment subjected to cyclic loading in uni-axial and bi-axial directions. We further demonstrate how the reorientation process of stress fibers is affected by an increasing cyclic load amplitude.

Modeling aspects: Experimental studies, performed on cells subjected to cyclic loading, usually involve a large number of samples [14, 47] followed by a statistical evaluation. To this end, the cell samples are placed on a substrate, which is kept inside a loading chamber subjected to cyclic loading and actin staining of stress fibers [48]. The statistical average of the experimental results is obtained and visualised through a circular histogram [47].

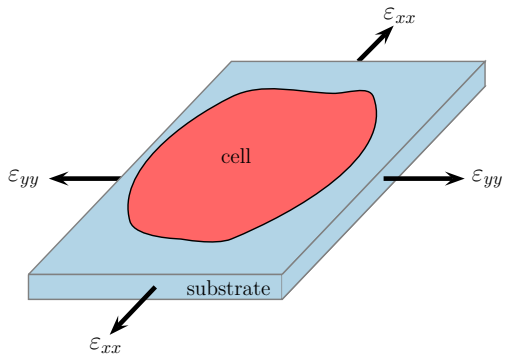

Figure 13: Cell placed on a substrate which is subjected to in-plane loading $\varepsilon_{ii}, i = x, y$, representing a strain loading applied on the substrate.

In the following study we model the 2D cell placed on a supporting substrate, cf. Fig. 13. A strain loading is applied to the substrate which leads to evaluating substrate stresses according to

$$\sigma_{ij}^{sub} \;=\; C_{ijkl}^{sub}\,\epsilon_{kl}^{0} \tag{45}$$

where C_{ijkl}^{sub} is the plane-stress elasticity tensor of the substrate and ϵ_{kl}^{0} is the applied strain in the substrate. The substrate stress is then added to the total stress, to update eq. (30) as

$$b\,\left(\Sigma_{ij} + \sigma_{ij}^{sub}\right)_{,j} \;=\; T_i\ . \tag{46}$$

Furthermore, we assume the computed results to qualitatively match the average experimental results. We consider 20 stress fiber orientations distributed uniformly between 0 and $\pi/2$. In accordance with the experiments the analysis results are presented with circular histograms in which the inclination of each line represents the corresponding stress fiber

orientation and the magnitude η represents the minimum value of the stress fiber concentration in that direction, over all elements. The model considers a quarter of the analysis domain using symmetry boundary conditions. The circular histogram domain between $\pi/2$ and 2π follows from the symmetry conditions.

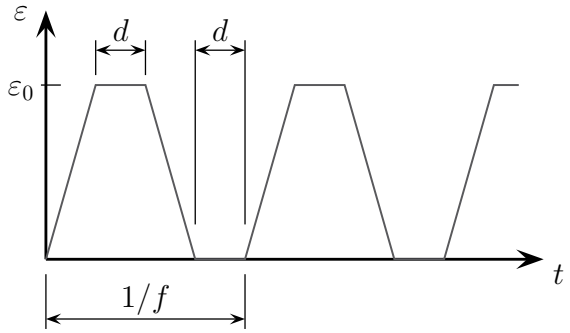

Figure 14: Principle cyclic stretch loading.

Recent in-vitro experiments studying the cell response to cyclic loading have revealed that the alignment of stress fibers within the cytoplasm may change depending on the type of loading and the substrate properties. A schematic diagram of an experimental set-up is shown in Fig. 13. The cell is placed on a substrate to which loading can be applied in all directions.

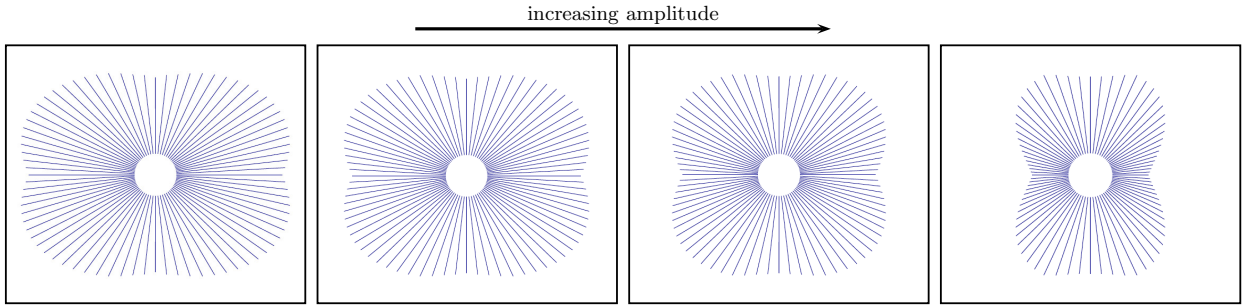

Figure 15: Stress fiber reorientation due to uni-axial loading in the horizontal direction. Alignment becomes significant with increasing amplitude.

In general, the reorientation of a cell follows the realignment of stress fibers but on a different time scale [48]. At equilibrium, the alignment of cells and stress fibers match each other, and hence the terminology cell and stress fiber reorientation, respectively, can be used interchangeably.

Direction of loading: In [47] it was observed that cells subjected to bi-axial loading do not exhibit a significant realignment while cells subjected to uniaxial loading do, which is usually termed *strain avoidance*. In a first analysis, we applied a horizontal uni-axial linear

triangular cyclic loading to the substrate, depicted in Fig. 14. The substrate has a stiffness of $20\,kPa$, Poisson ratio of 0.15 and all loading conditions were considered for uni-axial loading according to Table 2 in which d denotes a time span as defined in Fig. 14.

	frequency [mHz]	amplitude ε_0	d [s]
(a)	52	0.049	3
(b)	34	0.084	3
(c)	21	0.140	3
(d)	9	0.320	3

Table 2: Different applied cyclic loading conditions.

In Fig. 15 we show the results of the horizontal uni-axial loading in terms of circular histograms. With increasing load amplitude, the stress fibers increasingly realign in directions away from the loading direction. In our stress fiber model, the dissociation of stress fibers depends on the active stress. Thus, with increasing amplitude, the effect of dissociation is much more pronounced than the effect of association which matches the experimental observations presented in [48].
Generally, the active stress increases during the loading phase of a cycle and decreases during unloading. In Fig. 16 we observe a higher decrease of stress in the direction of loading than in the orthogonal direction. The figure shows the variation of the active stress for the last five loading cycles. The pronounced decrease of stress and the higher contractile strain results in a higher dissociation of stress fibers in loading direction. Thus, at equilibrium, the stress fiber concentration is lower in the direction of loading compared to the orthogonal direction.

Next, in order to study the realignment of stress fibers subjected to bi-axial loading, we apply the cyclic loading condition (d), cf. Table 2, in both, horizontal and vertical directions, keeping all the material parameters constant. The stress fiber orientation for such a bi-axial loading is shown in the circular histogram of Fig. 17. A strong contrast is observed between uni-axial loading and bi-axial loading for the same loading parameters. We can observe that, cells do not exhibit a preferred reorientation angle, when subjected to bi-axial loading as seen during the uni-axial loading.

Substrate stiffness: It has been observed experimentally that the properties of the substrate plays a prominent role in deciding the cellular reorientation response. In [48], it was observed that cells placed on substrates with stiffness values less than 11 kPa did not exhibit reorientation. In another set of experiments [14], it was shown that the stress fibers align along the direction of loading when the substrate was a soft collagen gel, and divert from the loading direction when the substrate is a stiff silicone rubber. In [17], stress fibers modeled as catch-bonds, also showed an increase of the contractile force with increasing substrate stiffness. To investigate this effect numerically, we placed the cell on the substrate and applied uni-axial cyclic loading as given in Fig. 14. Calculations were carried out for different

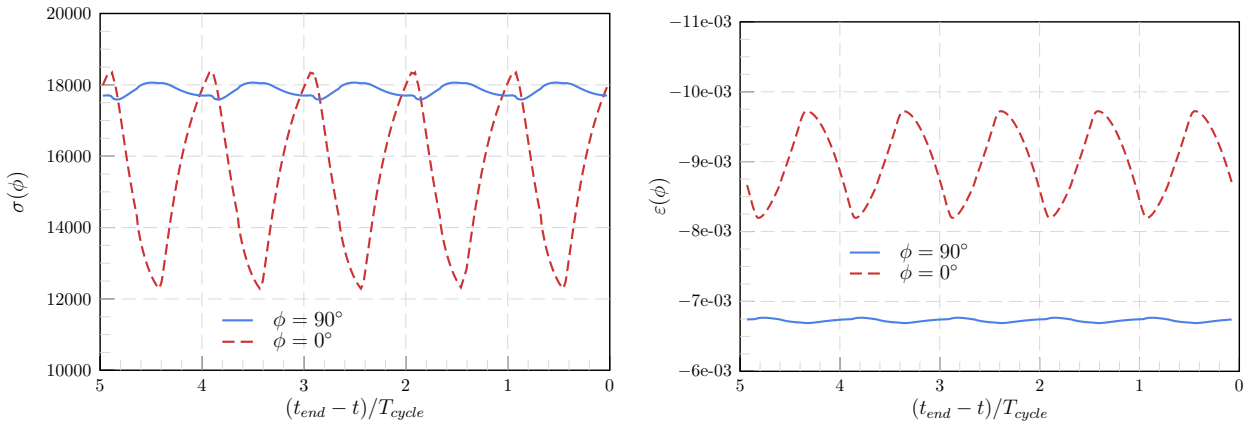

(a) stress **(b)** strain

Figure 16: Active stress in stress fibers along the loading and orthogonal directions and corresponding strain variation for the last five loading cycles.

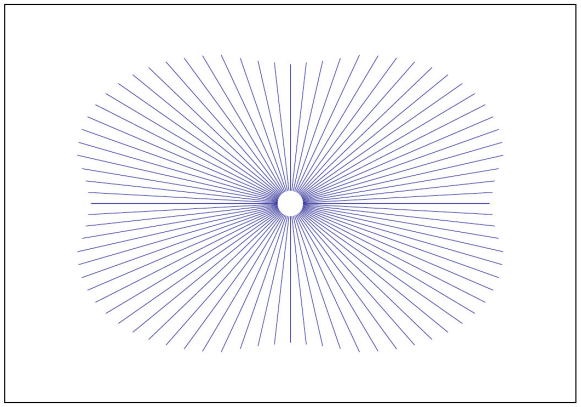

Figure 17: Stress fiber orientation due to bi-axial loading.

values of substrate stiffness while all other material parameters are held constant. We observe that the effect of applied cyclic loading becomes significant as the substrate stiffness increases, as seen in Fig. 18.

5. Summary and conclusions

We have presented a phenomenological model for the analysis of the chemo-mechanical response of contractile cells for static and cyclic loadings. We successfully simulated the coupling between focal adhesions and stress fibers through a feedback loop involving the cytoplasmic calcium concentration.

The key aspects can be summarized as follows:

- the stress fiber growth depends on the active stress in the stress fibers and the calcium

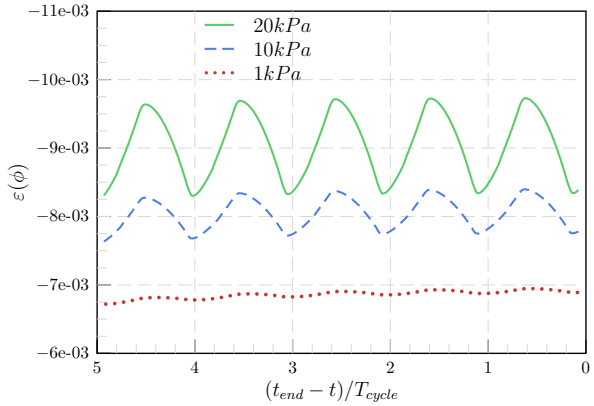

Figure 18: Strain in stress fibers at $\phi = 0$ for the last 5 loading cycles.

concentration. We exploited a smooth Hill-type model to simulate the growth of active stress within the stress fibers which directly affects their dissociation. Unlike in conventional models, mechanical equilibrium is ensured by including the substrate stress which is transferred from the loaded substrate to the cell domain.

- the calcium signal depends on the rate of formation of high affinity integrins or focal adhesion and the IP3 messenger molecule concentration in the cell. The focal adhesion model satisfies the thermodynamic equilibrium between the integrins. Different from the models presented in [36] and [27] the diffusion of low affinity integrins is not modeled explicitly since else the conservation of mass of the integrins is violated.
- the stress fiber formation is affected by the calcium concentration which changes the focal adhesion concentration. A mechanosensitive feedback loop in the calcium growth model is explicitly included in the simulations for the first time.
- the model follows a modular approach, where each section of the model can be replaced by an updated version without affecting other parts. We have solved the governing coupled system of equations with a monolithic approach where both, the mechanical equilibrium and the high affinity integrin growth, were solved simultaneously. This monolithic approach is highly stable regardless of the time step, thus providing an excellent quality of the solution. This is different from more conventional staggered solution schemes, which are often used in an attempt to simplify the solution, but where the quality of the solution can be adversely affected by the magnitude of the time step.

We have carried out various numerical tests to validate the principal model properties and have demonstrated the overall performance of our framework with several computational results. We have simulated successfully the contraction of 2D cells under the growth of focal adhesions and cells subjected to cyclic loading using a single set of parameters. We have also shown the importance of the calcium feedback loop in order to obtain the correct physics of the focal adhesion growth. Furthermore, we studied the influence of the cell supporting

substrate stiffness on the re-orientation process when the cell is subjected to cyclic loading. Recent experimental studies revealed the strong dependence of the stress fiber orientation on the substrate stiffness [49]. Hence, we believe that neglecting the substrate properties in the analysis model would spoil a reliable and accurate cell response. Consideration of the substrate stiffness in the model allows us to reveal systematically its impact on the strain variation in the stress fibers and showed virtually no effect for very low stiffness values of around $3\,kPa$. With increasing stiffness a re-orientation process started and showed a pronounced behavior for $> 11\,kPa$ where the stress fibers clearly started to orient away from the direction of cyclic stretching, which is in line with the experimental observations [48]. Finally, we observed that by increasing the amplitude of the cyclic loading, the effect of reorientation is increased.

In sum, we have formulated a robust model for the simulation of cell contractility and we have demonstrated the effects for a reliable and accurate numerical prediction of the chemo-mechanical cell response. The following aspects should be considered in future work: (i) the current model considers small strains which restricts its applicability to experiments. An extension to finite strains will significantly increase the set of validation test and will give further insight to large cell deformations. (ii) The current model assumes a perfect bond between the cell and the substrate which simplifies the transfer of stresses. A more sophisticated coupling which considers the true transfer mechanism through the focal adhesions will capture this mechanism. (iii) A set of experimental test is in preparation to provide evidence for selected aspects which support the development of independent models for focal adhesions and stress fibers.

Declaration of Interest:

Authors declare that they have no conflict of interest.

Appendix

The governing integral equations of the chemo-mechanical equilibrium are:

$$-b \int_{\Omega_e} \left(\sigma_{ij} + C_{ijkl}\, \varepsilon_{kl}\right) \left(\delta u_{i,j}\right) dA - \int_{\Omega_e} \xi_H\, F_i \left(\delta u_i\right) dA \;=\; 0. \tag{47}$$

Discretization of the solution domain in terms of finite elements using the interpolation

approach, eq. (41) and eq. (42), replaces eq. (47) with the governing algebraic equations:

$$\delta\mathbf{U}^T b \sum_e \left\{ \int_{\Omega_e} \mathbf{B}^T \mathbf{C}\, \mathbf{B}\, dA \right\} \mathbf{U} + \delta\mathbf{U}^T \sum_e \left\{ \int_{\Omega_e} \mathbf{R}_u^T \mathbf{F}\, \mathbf{R}_\xi\, dA \right\} \mathbf{\Xi}_H$$
$$= -\delta\mathbf{U}^T b \sum_e \left\{ \int_e \mathbf{B}^T \boldsymbol{\sigma} dA \right\} \tag{48}$$

where b denotes the cell thickness, $\mathbf{R}_u$ and $\mathbf{R}_\xi$ denote the element shape function vector to interpolate the unknown nodal displacements and high affinity integrin concentrations, respectively. Matrix $\mathbf{B}$ interpolates the strain coordinates and contains derivatives of the shape functions of eq. (41) with respect to the global coordinates.

Similarly, the weak form for the conservation of the number of integrins:

$$b \int_{\Omega_e} \xi_H\, (\delta\, \xi_H)\, dA - b \int_{\Omega_e} \frac{\xi_0\, \alpha}{1+\alpha}\, (\delta\, \xi_H)\, dA = 0 \tag{49}$$

is replaced by the discrete form:

$$\delta\mathbf{\Xi}^T b \sum_e \left\{ \int_{\Omega_e} \mathbf{R}_u\, \mathbf{R}_\xi^T\, dA \right\} \mathbf{\Xi} = \delta\mathbf{\Xi}^T b \sum_e \left\{ \int_{\Omega_e} \frac{\xi_0\, \alpha}{1+\alpha} \mathbf{R}_\xi\, dA \right\}. \tag{50}$$

From the discrete equations (48) and (50) follow the element contributions which are assembled into the governing monolithic system of equations, cf eq. (43):

$$\mathbf{K}_{UU} = b \int_{\Omega_e} \mathbf{B}^T \mathbf{C}\, \mathbf{B}\, dA \tag{51}$$

$$\mathbf{K}_{U\Xi} = \int_{\Omega_e} \mathbf{R}_u^T \mathbf{F}\, \mathbf{R}_\xi\, dA \tag{52}$$

$$\mathbf{K}_{\Xi\Xi} = b \int_{\Omega_e} \mathbf{R}_\xi^T \mathbf{R}_\xi\, dA \tag{53}$$

$$\mathbf{F}_U = -b \int_{\Omega_e} \mathbf{B}^T \boldsymbol{\sigma}\, dA \tag{54}$$

$$\mathbf{F}_\Xi = b \int_{\Omega_e} \frac{\xi_0\, \alpha}{1+\alpha} \mathbf{R}_\xi\, dA \tag{55}$$

The weak form for the IP3 diffusion, equation (36)

$$\int_\Omega \dot{S}(\delta S)\, dA = -\, m_s\, k\, T \int_\Omega \frac{\partial S}{\partial x_i} \frac{\partial(\delta S)}{\partial x_i}\, dA - k_d \int_\Omega S\, (\delta S)\, dA - \dot{\varepsilon} \int_\Omega S\, (\delta S)\, dA$$
$$+ \frac{\alpha_c}{b}\, max(0, \dot{\xi}_H) \int_\Omega \delta S\, dA \tag{56}$$

involves the time derivative of the IP3 concentration (S) which is discretized as

$$\dot{S} = \frac{S - S^t}{\Delta t} \quad . \tag{57}$$

Substituting equation (57) into (56) provides,

$$\int_\Omega \frac{S - S^t}{\Delta t}(\delta S)\, dA = - m_s\, k\, T \int_\Omega \frac{\partial S}{\partial x_i}\frac{\partial (\delta S)}{\partial x_i}\, dA - k_d \int_\Omega S\,(\delta S)\, dA - \dot{\varepsilon} \int_\Omega S\,(\delta S)\, dA + \frac{\alpha_c}{b}\, max(0, \dot{\xi}_H) \int_\Omega \delta S\, dA \tag{58}$$

which has the discrete form:

$$\sum_e \left\{ \frac{1}{\Delta t} \int_{\Omega_e} \mathbf{R}_s^T \mathbf{R}_s\, dA \;+\; m_s k T \int_{\Omega_e} \mathbf{B^T B}\, dA + k_d \int_{\Omega_e} \mathbf{R}_s{}^T \mathbf{R}_s\, dA + \dot{\varepsilon} \int_{\Omega_e} \mathbf{R}_s^T \mathbf{R_s}\, dA \right\} \mathbf{S} = \sum_e \left\{ \frac{1}{\Delta t} \int_{\Omega_e} S^t \mathbf{R}_s^T\, dA + \int_{\Omega_e} \frac{\alpha}{b} \max(0, \dot{\xi}_H) \mathbf{R}_s^T\, dA \right\} \tag{59}$$

where $\mathbf{R}_s$ denotes the element shape function vector to interpolate the unknown IP3 concentration. Matrix $\mathbf{B}$ interpolates the strain coordinates and contains derivatives of the shape functions of eq. (39) with respect to the global coordinates. The element stiffness matrix follows as

$$\mathbf{K}_{ss} = \left\{ \frac{1}{\Delta t} \int_{\Omega_e} \mathbf{R}_s^T \mathbf{R}_s\, dA \;+\; m_s k T \int_{\Omega_e} \mathbf{B^T B}\, dA + k_d \int_{\Omega_e} \mathbf{R}_s{}^T \mathbf{R}_s\, dA + \dot{\varepsilon} \int_{\Omega_e} \mathbf{R}_s^T \mathbf{R_s}\, dA \right\} \tag{60}$$

References

[1] G. Bao, S. Suresh, Cell and molecular mechanics of biological materials, Nature materials 2 (11) (2003) 715–725. doi:10.1038/nmat1001.

[2] B. Cooke, N. Mohandas, R. Coppel, The malaria-infected red blood cell: Structural and functional changes, Vol. 50, Academic Press, 2001, pp. 1–86, dOI: 10.1111/j.1365-2141.2011.08755.x.

[3] L. Chin, Y. Boss, C. Pascoe, T. Hackett, C. Seow, P. Par, Mechanical properties of asthmatic airway smooth muscle, European Respiratory Journal 40 (1) (2012) 45–54. doi:10.1183/09031936.00065411.

[4] J. Guck, S. Schinkinger, B. Lincoln, F. Wottawah, S. Ebert, M. Romeyke, D. Lenz, H. M. Erickson, R. Ananthakrishnan, D. Mitchell, J. Ks, S. Ulvick, C. Bilby, Optical Deformability as an Inherent Cell

Marker for Testing Malignant Transformation and Metastatic Competence, Biophysical Journal 88 (5) (2005) 3689–3698. doi:10.1529/biophysj.104.045476.

[5] B. Alberts, A. Johnson, J. Lewis, M. Raff, K. Roberts, P. Walter, Molecular Biology of the Cell, 4th Edition, Garland Science, 2002.

[6] L. J. Peterson, Z. Rajfur, A. S. Maddox, C. D. Freel, Y. Chen, M. Edlund, C. Otey, K. Burridge, Simultaneous Stretching and Contraction of Stress Fibers In Vivo, Molecular Biology of the Cell 15 (7) (2004) 3497–3508. doi:10.1091/mbc.E03-09-0696.

[7] S. K. Sastry, K. Burridge, Focal Adhesions: A Nexus for Intracellular Signaling and Cytoskeletal Dynamics, Experimental Cell Research 261 (1) (2000) 25–36. doi:10.1006/excr.2000.5043.

[8] G. Binnig, C. F. Quate, C. Gerber, Atomic Force Microscope, Physical Review Letters 56 (9) (1986) 930–933. doi:10.1103/PhysRevLett.56.930.

[9] R. M. Hochmuth, Micropipette aspiration of living cells, Journal of Biomechanics 33 (1) (2000) 15–22. doi:10.1016/S0021-9290(99)00175-X.

[10] J. D. Mih, A. Marinkovic, F. Liu, A. S. Sharif, D. J. Tschumperlin, Matrix stiffness reverses the effect of actomyosin tension on cell proliferation, Journal of Cell Science 125 (24) (2012) 5974–5983. doi:10.1242/jcs.108886.

[11] C. E. Chan, D. J. Odde, Traction Dynamics of Filopodia on Compliant Substrates, Science 322 (5908) (2008) 1687–1691. doi:10.1126/science.1163595.

[12] Y. Cui, F. M. Hameed, B. Yang, K. Lee, C. Q. Pan, S. Park, M. Sheetz, Cyclic stretching of soft substrates induces spreading and growth, Nature Communications 6 (2015) 6333. doi:10.1038/ncomms7333.

[13] R. Kaunas, P. Nguyen, S. Usami, S. Chien, Cooperative effects of Rho and mechanical stretch on stress fiber organization, Proceedings of the National Academy of Sciences of the United States of America 102 (44) (2005) 15895–15900. doi:10.1073/pnas.0506041102.

[14] A. Tondon, H.-J. Hsu, R. Kaunas, Dependence of cyclic stretch-induced stress fiber reorientation on stretch waveform, Journal of Biomechanics 45 (5) (2012) 728–735. doi:10.1016/j.jbiomech.2011.11.012.

[15] D. E. Ingber, Cellular tensegrity: defining new rules of biological design that govern the cytoskeleton, Journal of Cell Science 104 (Pt 3) (1993) 613–627.

[16] R. L. Satcher, C. F. Dewey, Theoretical estimates of mechanical properties of the endothelial cell cytoskeleton, Biophysical Journal 71 (1) (1996) 109–118. doi:10.1016/S0006-3495(96)79206-8.

[17] F. J. Vernerey, U. Akalp, Role of catch bonds in actomyosin mechanics and cell mechanosensitivity, Physical Review E 94 (1). doi:10.1103/PhysRevE.94.012403.
URL `https://link.aps.org/doi/10.1103/PhysRevE.94.012403`

[18] U. Akalp, C. Schnatwinkel, M. P. Stoykovich, S. J. Bryant, F. J. Vernerey, Structural Modeling of Mechanosensitivity in Non-Muscle Cells: Multiscale Approach to Understand Cell Sensing, ACS Biomaterials Science & Engineeringdoi:10.1021/acsbiomaterials.6b00693.
URL `http://pubs.acs.org/doi/abs/10.1021/acsbiomaterials.6b00693`

[19] V. S. Deshpande, R. M. McMeeking, A. G. Evans, A bio-chemo-mechanical model for cell contractility, Proceedings of the National Academy of Sciences 103 (38) (2006) 14015–14020. doi:10.1073/pnas.0605837103.

[20] F. J. Vernerey, M. Farsad, A constrained mixture approach to mechano-sensing and force generation in contractile cells, Journal of the Mechanical Behavior of Biomedical Materials 4 (8) (2011) 1683–1699. doi:10.1016/j.jmbbm.2011.05.022.

[21] C. Obbink-Huizer, C. W. J. Oomens, S. Loerakker, J. Foolen, C. V. C. Bouten, F. P. T. Baaijens, Computational model predicts cell orientation in response to a range of mechanical stimuli, Biomechanics and Modeling in Mechanobiology 13 (1) (2014) 227–236. doi:10.1007/s10237-013-0501-4.

[22] A. Vigliotti, W. Ronan, F. P. T. Baaijens, V. S. Deshpande, A thermodynamically motivated model for stress-fiber reorganization, Biomechanics and Modeling in Mechanobiology 15 (4) (2015) 761–789. doi:10.1007/s10237-015-0722-9.

[23] C. Zhu, G. Bao, N. Wang, Cell Mechanics: Mechanical Response, Cell Adhesion, and Molecular Deformation, Annual Review of Biomedical Engineering 2 (1) (2000) 189–226. doi:10.1146/annurev.bioeng.2.1.189.

[24] Z. Wei, V. S. Deshpande, R. M. McMeeking, A. G. E. Evans, Analysis and Interpretation of Stress Fiber Organization in Cells Subject to Cyclic Stretch, Journal of Biomechanical Engineering 130 (3) (2008) 031009. doi:10.1115/1.2907745.
[25] V. S. Deshpande, Analysis and Interpretation of Stress Fiber Organization in Cells Subject to Cyclic Stretch, Journal of Biomechanical Engineering 130 (3) (2008) 031009. doi:10.1115/1.2907745.
[26] A. Pathak, R. M. McMeeking, A. G. Evans, V. S. Deshpande, An Analysis of the Cooperative Mechano-Sensitive Feedback Between Intracellular Signaling, Focal Adhesion Development, and Stress Fiber Contractility, Journal of Applied Mechanics 78 (4) (2011) 041001. doi:10.1115/1.4003705.
[27] F. J. Vernerey, M. Farsad, A mathematical model of the coupled mechanisms of cell adhesion, contraction and spreading, Journal of Mathematical Biology 68 (4) (2014) 989–1022. doi:10.1007/s00285-013-0656-8.
[28] A. Besser, S. A. Safran, Force-Induced Adsorption and Anisotropic Growth of Focal Adhesions, Biophysical Journal 90 (10) (2006) 3469–3484. doi:10.1529/biophysj.105.074377.
[29] T. Shemesh, B. Geiger, A. D. Bershadsky, M. M. Kozlov, Focal adhesions as mechanosensors: A physical mechanism, Proceedings of the National Academy of Sciences of the United States of America 102 (35) (2005) 12383–12388. doi:10.1073/pnas.0500254102.
[30] S. Pellegrin, H. Mellor, Actin stress fibres, Journal of Cell Science 120 (20) (2007) 3491–3499. doi:10.1242/jcs.018473.
[31] W. Goldmann, G. Isenberg, Analysis of filamin and -actinin binding to actin by the stopped flow method, FEBS Letters 336 (3) (1993) 408–410. doi:10.1016/0014-5793(93)80847-N.
[32] G. Holzapfel, J. Wehland, K. Weber, Calcium control of actin-myosin based contraction in triton models of mouse 3t3 fibroblasts is mediated by the myosin light chain kinase (MLCK)-calmodulin complex, Experimental Cell Research 148 (1) (1983) 117–126. doi:10.1016/0014-4827(83)90192-1.
[33] K. Hirata, A. Kikuchi, T. Sasaki, S. Kuroda, K. Kaibuchi, Y. Takai, Involvement of tho p21 in the GTP-enhanced Calcium Ion Sensitivity of Smooth Muscle Contraction, Journal of Biological Chemsitry 267 (1992) 8719–8722.
[34] J. T. Herlihy, R. A. Murphy, Length-Tension Relationship of Smooth Muscle of the Hog Carotid Artery, Circulation Research 33 (3) (1973) 275–283. doi:10.1161/01.RES.33.3.275.
[35] A. V. Hill, The Heat of Shortening and the Dynamic Constants of Muscle, Proceedings of the Royal Society of London B: Biological Sciences 126 (843) (1938) 136–195. doi:10.1098/rspb.1938.0050.
[36] V. S. Deshpande, M. Mrksich, R. M. Mcmeeking, A. Evans, A bio-mechanical model for coupling cell contractility with focal adhesion formation, Journal of the Mechanics and Physics of Solids 56 (4) (2008) 1484–1510. doi:10.1016/j.jmps.2007.08.006.
[37] H. Murakoshi, H. Wang, R. Yasuda, Local, persistent activation of Rho GTPases during plasticity of single dendritic spines, Nature 472 (7341) (2011) 100–104. doi:10.1038/nature09823.
[38] K. Bhadriraju, M. Yang, S. Alom Ruiz, D. Pirone, J. Tan, C. S. Chen, Activation of ROCK by RhoA is regulated by cell adhesion, shape, and cytoskeletal tension, Experimental Cell Research 313 (16) (2007) 3616–3623. doi:10.1016/j.yexcr.2007.07.002.
[39] M. Schwartz, Rho signalling at a glance, Journal of Cell Science 117 (23) (2004) 5457–5458. doi:10.1242/jcs.01582.
[40] M. A. Wozniak, K. Modzelewska, L. Kwong, P. J. Keely, Focal adhesion regulation of cell behavior, Biochimica et Biophysica Acta (BBA) - Molecular Cell Research 1692 (2-3) (2004) 103–119. doi:10.1016/j.bbamcr.2004.04.007.
[41] X.-D. Ren, R. Wang, Q. Li, L. A. F. Kahek, K. Kaibuchi, R. A. F. Clark, Disruption of Rho signal transduction upon cell detachment, Journal of Cell Science 117 (16) (2004) 3511–3518. doi:10.1242/jcs.01205.
[42] T. Meyer, L. Stryer, Molecular model for receptor-stimulated calcium spiking, Proceedings of the National Academy of Sciences 85 (14) (1988) 5051–5055.
[43] W. Press, S. Teukolsky, W. Vetterling, B. Flannery, Numerical Recipes - The Art of Scientific Computing, 3rd Edition, Cambridge University Press, 2007.
[44] C. G. Galbraith, K. M. Yamada, M. P. Sheetz, The relationship between force and focal complex development, The Journal of Cell Biology 159 (4) (2002) 695–705. doi:10.1083/jcb.200204153.

[45] N. Q. Balaban, U. S. Schwarz, D. Riveline, P. Goichberg, G. Tzur, I. Sabanay, D. Mahalu, S. Safran, A. Bershadsky, L. Addadi, others, Force and focal adhesion assembly: a close relationship studied using elastic micropatterned substrates, Nature cell biology 3 (5) (2001) 466–472.

[46] C. S. Chen, J. L. Alonso, E. Ostuni, G. M. Whitesides, D. E. Ingber, Cell shape provides global control of focal adhesion assembly, Biochemical and Biophysical Research Communications 307 (2) (2003) 355–361. doi:10.1016/S0006-291X(03)01165-3.

[47] R. Kaunas, S. Usami, S. Chien, Regulation of stretch-induced JNK activation by stress fiber orientation, Cellular Signalling 18 (11) (2006) 1924–1931. doi:10.1016/j.cellsig.2006.02.008.

[48] U. Faust, N. Hampe, W. Rubner, N. Kirchge\s sner, S. Safran, B. Hoffmann, R. Merkel, Cyclic Stress at mHz Frequencies Aligns Fibroblasts in Direction of Zero Strain, PLoS ONE 6 (12) (2011) e28963. doi:10.1371/journal.pone.0028963.

[49] A. Tondon, R. Kaunas, The Direction of Stretch-Induced Cell and Stress Fiber Orientation Depends on Collagen Matrix Stress, PLoS ONE 9 (2) (2014) e89592. doi:10.1371/journal.pone.0089592.